

Lagrangian transport and chaos in the near wake of the flow around an obstacle: a numerical implementation of lobe dynamics

J. Duan¹ and S. Wiggins^{2,*}

¹Department of Mathematical Sciences, Clemson University, Clemson, South Carolina 29634

²Control and Dynamical Systems, 107-81, Caltech, Pasadena, CA 91125

*This research was supported by ONR Grant No. N00014-97-1-0071

Received 27 May 1997 – Accepted: 3 April 1998

Abstract. In this paper we study Lagrangian transport in the near wake of the flow around an obstacle, which we take to be a cylinder. In this case, for the range of Reynolds numbers investigated, the flow is two-dimensional and time periodic. We use ideas and methods from transport theory in dynamical systems to describe and quantify transport in the near wake. We numerically solve the Navier-Stokes equations for the velocity field and apply these methods to the resulting numerical representation of the velocity field. We show that the method of lobe dynamics can be used in conjunction with computational fluid dynamics methods to give very detailed and quantitative information about Lagrangian transport. In particular, we show how the stable and unstable manifolds of certain saddle-type stagnation points on the cylinder, and one in the wake, can be used to divide the flow into three distinct regions, an upper wake, a lower wake, and a wake cavity. The significance of the division using stable and unstable manifolds lies in the fact that these invariant manifolds form a template on which the transport occurs. Using this, we compute fluxes from the upper and lower wakes into the wake cavity using the associated turnstile lobes. We also compute escape time distributions as well as compare transport properties for two different Reynolds numbers.

fluid particle paths take the form of Hamilton's canonical equations with the streamfunction playing the role of the Hamiltonian function. If the flow is time-periodic, then the study of fluid particle trajectories can be reduced to the study of an associated two-dimensional, area-preserving Poincaré map. In this setting many techniques of dynamical systems theory can be immediately applied. Moreover, they have immediate implications for fluid transport issues. For example, KAM tori are barriers to the transport of fluid and Smale horseshoes give rise to chaotic fluid particle paths and rapid mixing. Essentially all of this work has been in the situation where one has an explicit analytical formula for the velocity field. From the point of view of applications, this is a severe limitation, and this is where computational fluid dynamics enters the picture.

Over the past 15 years computational fluid dynamics has developed into a subject in its own right. Now we have accurate algorithms for solving the Navier Stokes equations in a variety of physically important settings. However, many problems related to mixing and transport begin once this step has been accomplished. That is, first a solution to the Navier Stokes equations must be obtained in order to study the transport and mixing properties associated with that velocity field. In the vast majority of situations arising in applications, this solution can only be obtained numerically. Thus, we only have a numerical representation of the vector field. Nevertheless, most dynamical systems results are not dependent on a specific analytical form of the dynamical system under consideration. Rather, they require that only certain *geometrical features* be present. For example, the existence of stable and unstable manifolds of some invariant set requires only the existence of a hyperbolic invariant set, the existence of Smale horseshoe type chaos requires only the transverse intersection of the stable and unstable manifolds of a hyperbolic periodic orbit, and the existence of KAM tori requires only that the flow be a two-dimensional time-periodic

1 Introduction

There has been much work on applying dynamical systems techniques to the study of mixing and transport issues in fluids over the past 10 years. Babiano et al. [1994] and Aref and El Naschie [1994] provide recent reviews. However, most of this work has been done in the context of two-dimensional, time-periodic flows. There is good reason for this. In this situation the equations for

Correspondence to: S. Wiggins

perturbation of an integrable flow that has a region of closed streamlines. If it is known that these structures are present in the flow, then this information, along with information on their geometrical arrangement in the flow, can be used to gain a quantitative understanding of transport. For example, if a flow with periodic boundary conditions contains a KAM torus then recent work of Mezić and Wiggins [1994] shows that, neglecting molecular diffusion, an initial distribution of tracer that is both inside and outside the KAM torus will exhibit asymptotic t^2 dispersion. If the effects of molecular diffusion are considered then work of Mezić et al. [1996] shows that in the high Peclet number limit the effective diffusivity scales like the square of the Peclet number. The existence of a Smale horseshoe implies the existence of *local* exponential expansion of fluid line elements and rapid stirring of fluid. The stable and unstable manifolds of hyperbolic periodic orbits may form a template which governs large scale transport in a flow (Beigie et al. [1994]). A common feature of each of these examples is that a “low dimensional” geometric feature of the flow can be used to quantify a more global feature of the transport.

Because of the current limitations in the applications of these methods (i.e. the need for an analytical representation of the velocity field) a useful area of research is the development of dynamical systems techniques for the analysis of numerical representations of velocity fields. In this paper we consider transport in the wake of the flow around bluff bodies. In particular, we have considered the flow around a cylinder. Our work is a continuation of earlier work of Shariff et al. [1991] who showed that dynamical systems theory could be used to explain a variety of observations related to the flow in the near wake of a cylinder due to Perry et al. [1982].

There are several reasons that make this flow an ideal starting point for the development of dynamical systems techniques for the analysis of Lagrangian transport properties numerical representations of velocity fields. One is that for Reynolds numbers smaller than about 190 the flow is experimentally well-established to be two-dimensional. For Reynolds numbers larger than about 50 it is also time-periodic. Thus we are in a situation where the mathematical *theory* is well-developed, but its implementation for numerical velocity fields is not. Moreover, the numerical computation of the flow around a cylinder for this range of Reynolds numbers is standard. Thus we are also in a situation where we can concentrate solely on the development of dynamical systems techniques for analyzing numerical velocity fields without having to develop new dynamical systems theory or deal with computational issues arising from the first step of solving the Navier-Stokes equations. In this paper we consider two Reynolds numbers: 100 and 190. Reynolds number 100 puts us in the middle of the Reynolds number range where the

flow is well-established to be two-dimensional and time-periodic. Reynolds number 190 is very close to the critical number where a three-dimensional instability occurs. For both Reynolds numbers there are five stagnation points of interest in the flow: four on the cylinder and one in the wake. We have shown that the stable and unstable manifolds of these stagnation points (one dimensional curves) form a template which governs the process of Lagrangian transport in, and near, the wake. Most importantly, we have computed these manifolds from the numerical solution of the Navier-Stokes equations for flow around the cylinder.

As mentioned earlier, our work is a continuation of the work of Shariff et al. [1991]. Their paper laid the foundation for the dynamical systems analysis for fluid transport in the near wake of a cylinder in the time-periodic regime. Through comparisons with experimental observations of Perry et al. [1982], they argued that dynamical systems theory provided an excellent framework for considering a variety of transport issues from the Lagrangian point of view. An important contribution was an analytical argument for finding (non-hyperbolic¹) stagnation points on the cylinder having stable or unstable manifolds. They also gave a detailed discussion of the numerical issues for locating such points, as well as tracking particle trajectories generated by a numerically obtained velocity field. They locate the stagnation points on the circular cylinder surface with unstable or stable manifolds as well as locate a hyperbolic periodic point in the wake and generate its unstable and stable manifolds. From this information they determine the manner in which the manifolds divide the flow into an upper wake, lower wake, and a wake cavity. They also constructed the turnstile lobes associated with transport between the upper wake and the wake cavity and those associated with transport between the lower wake and wake cavity.

We carry on the analysis from this point using the manifolds, and the numerical implementation of the technique of *lobe dynamics*. This allows us to go further and show the following.

- We have computed areas of the turnstile lobes associated with transport. The area of the respective turnstile lobes gives us the flux between the upper wake and the wake cavity and the flux between the lower wake and wake cavity.
- We have shown that once particles leave the wake cavity they cannot return to the wake cavity (up to the limit of the time of computation).
- We have shown that the only way that particles can move from the upper (resp. lower) wake into

¹Following the terminology of dynamical systems theory, a stagnation point is said to be *hyperbolic* if the matrix associated with the linearization of the velocity field about the stagnation point has no eigenvalues on the imaginary axis.

the lower (resp. upper) wake is by making an intermediate passage through the wake cavity.

- We have determined the percentage of particles entrained into the wake cavity from the upper wake that escape from the wake cavity on successive shedding cycles.
- We have shown that for Reynolds number 100 essentially no “cross-wake” transport (i.e., transport from the upper to lower wake, and vice-versa) occurs while for Reynolds number 190 substantial cross-wake transport occurs. This was also noted by Shariff et al. [1991]. The reason for this is that in the former case there is an “almost” heteroclinic connection that acts as a barrier to transport.
- We have numerically implemented a topological argument that indicates that the wake cavity contains a Smale horseshoe type invariant set that gives rise to chaotic particle trajectories and associated exponential expansion of fluid line elements.

Hence, dynamical systems techniques, and lobe dynamics in particular, can be used in conjunction with techniques in computational fluid dynamics to give very detailed information about Lagrangian transport.

2 The Velocity Field

We obtain the velocity field $u(x, y, t), v(x, y, t)$ for flow past a circular cylinder from time-dependent simulations of the incompressible Navier-Stokes equations on a two-dimensional rectangular domain via a spectral element method. For background on the method see Patera [1984], Fischer [1989] and references therein. The actual data for the velocity field used in this paper is generated on a multiprocessor Silicon Graphics machine by an unstructured spectral element program developed in Henderson [1994] and Henderson and Karniadakis [1995].

Our computation is based on a circular cylinder with diameter 1. At the left, upper and lower boundaries of a rectangular computational domain, we use a uniform flow boundary condition: $u = 1, v = 0$. At the right boundary, we use a standard outflow boundary condition for the velocity and pressure (p):

$$\partial u / \partial x = 0, \quad \partial v / \partial x = 0, \quad p = 0.$$

At the surface of the cylinder we apply no-slip boundary conditions. The simulations are run long enough to obtain an asymptotic, time-periodic velocity field.

2.1 Particle Paths

The fluid particle motions are governed by

$$\dot{x} = u(x, y, t), \tag{1}$$

$$\dot{y} = v(x, y, t). \tag{2}$$

The velocity field $u(x, y, t), v(x, y, t)$ is interpolated by bicubic splines and particle paths or trajectories are obtained by solving (1)-(2). The velocity field obtained in this way remains incompressible up to some computational precision. We discuss a test of this later after we have introduced the idea of “turnstile lobes” and computed their area.

The particle trajectories are solved using a fourth order Runge-Kutta scheme, and these trajectories are visualized by a graphical user interface developed by Shariff and Pulliam. When the velocity field is periodic in time, we can locate fixed points of the associated Poincaré map (see the next section). By iterating line or curve segments sufficiently close to the fixed points, we can generate good approximations to the stable and unstable manifolds emanating from such fixed points. To plot the various manifolds we use the commercial data processing tool TECPLOT.

2.2 The Poincaré Map

For time-periodic velocity fields a variety of standard dynamical systems techniques and results make it advantageous to consider particle kinematics via the so called *Poincaré map*, which we will denote by P . That is, rather than plotting a particle trajectory as a continuous curve in space one plots its evolution at discrete intervals of time, where the interval of time is equal to the period of the velocity field. Thus, it is important to keep in mind that for the Poincaré map particle trajectories are manifested as sequences of discrete points (called *orbits*), rather than continuous curves.

For Reynolds numbers 100 and 190 there are five saddle-type fixed points associated with the cylinder that will be of interest; four on the cylinder and one in the wake. The points on the cylinder are characterized by zero time-averaged tangential shear stress (Shariff et al. [1991]) and each has associated with it an *invariant curve*. In Fig. 1 we illustrate these points along with a small piece of the associated invariant curves.

Invariant means that trajectories with initial conditions on the curve always remain on the curve. Consequently these invariant curves provide barriers to fluid transport in much the same way that streamlines do for *steady* two-dimensional flows. In dynamical systems jargon the invariant curves associated with the points at the front and back of the cylinder are referred to as *stable manifolds* since trajectories on these curves approach the saddle points asymptotically as time approaches $+\infty$. The invariant curves associated with each of the other two points at the back of the cylinder are referred to as *unstable manifolds* since trajectories on these curves approach the saddle points asymptotically as time approaches $-\infty$. The saddle point in the wake has both stable and unstable manifolds.

For unsteady flows the stable and unstable manifolds of different saddle-type fixed points may not coincide (or

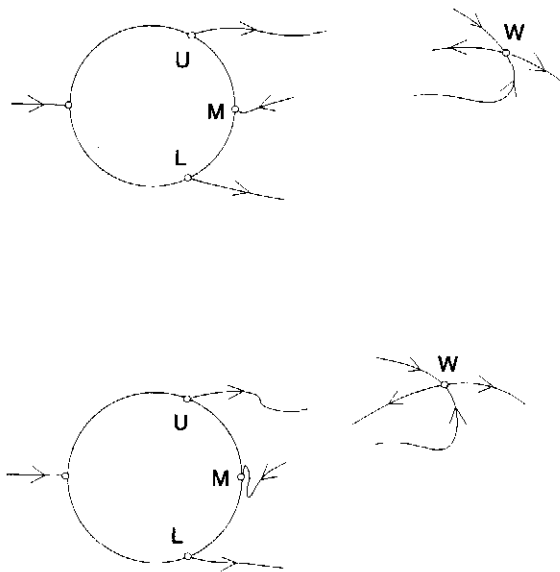


Fig. 1. $Re = 100$ (top) and $Re = 190$ (bottom): The five saddle points and small pieces of their associated invariant curves.

“join up”) to make a separatrix of finite length, rather they may intersect in a discrete number of points and wind throughout the flow as illustrated in Fig. 2. (The stable and unstable manifolds of the different saddle-type fixed points actually have infinite length, but we obviously can only show a finite portion of each in the figure.) Next we consider transport in the near wake and show how the geometric structure associated with the stable and unstable manifolds of the different saddle-type fixed points influence transport.

3 Transport in the Near Wake: Turnstiles and Lobe Dynamics

3.1 The Steady Wake: No Transport

To motivate our study of transport in the near wake of a circular cylinder, we first consider the case of a steady wake. For Reynolds numbers Re approximately between 5 and 41, the flow past a circular cylinder is steady, separated and with standing eddies (Van Dyke [1982]). We sketch the streamline pattern below for $Re = 40$, based on the numerical simulation of Dennis and Chang [1970].

We note that there are five stagnation points. The flow is divided by streamlines into an upper wake, a wake cavity and a lower wake. The wake cavity is *symmetric* with respect to a horizontal line through the center of the cylinder and it is further divided into two identical

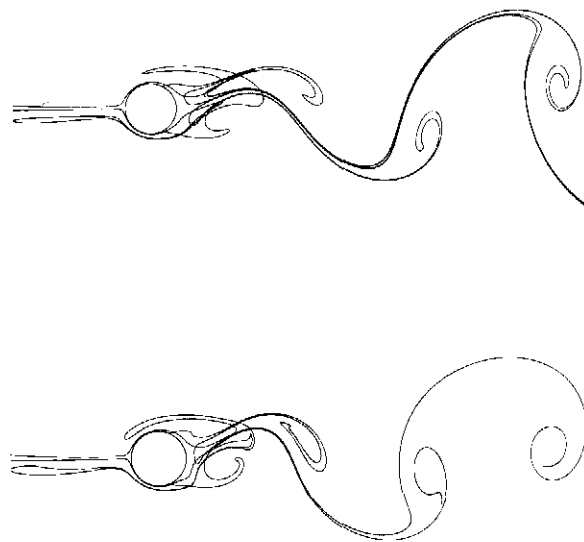


Fig. 2. $Re = 100$ (top) and $Re = 190$ (bottom): “Tangling” of the stable and unstable manifolds of the saddle-type fixed points associated with the Poincaré map.

“cells”, i.e., an upper cavity and a lower cavity.

Since fluid particles move along streamlines in this steady flow, it is clear that there is no fluid transport between upper wake and wake cavity, or between lower wake and wake cavity. There is also no cross wake transport. However, for an unsteady wake, we will see that the situation is very different.

3.2 The Division of the Flow into Regions

For the Poincaré map, segments of finite length of the stable and unstable manifolds of the saddle-type fixed points can be used to form boundaries between regions in the flow corresponding to qualitatively different particle trajectories. We illustrate this in Fig. 4 where the segments of finite length begin at the saddle-type fixed points denoted U and L and end at particular intersec-

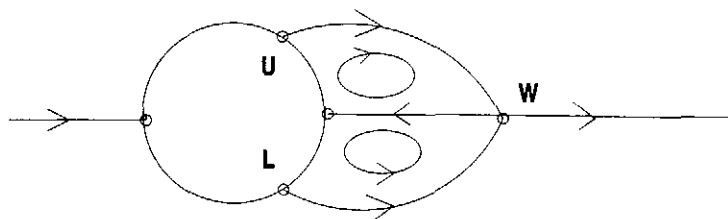


Fig. 3. $Re = 40$: Sketch of the streamline pattern based on the numerical simulation by Dennis and Chang [1970].

tion points of the stable and unstable manifolds, which we will refer to as the *boundary intersection points* (the choice of which is arbitrary), labelled q_1 and q_2 in the figure. In the figure we continue drawing the manifolds only slightly past the boundary intersection points so that the boundaries we are considering are clearly illustrated.

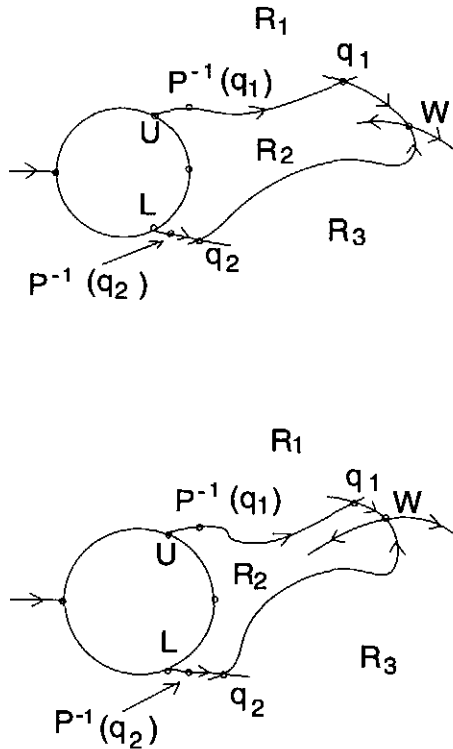


Fig. 4. $Re = 100$ (top) and $Re = 190$ (bottom): Boundaries made up of segments of stable and unstable manifolds between different regions for the Poincaré map of the cylinder flow.

The curves depicted in Fig. 4 bound three regions: the upper wake (R_1), the lower wake (R_3), and the wake cavity (R_2). We remark that the wake cavity is generally not symmetric with respect to a horizontal line through the center of the cylinder, and this is quite different from the wake cavity in the steady wake as shown in Fig. 3. Understanding the reasons for this would require a study of the spatial variation of the time dependence, which is beyond the scope of this paper. However, the wake cavity is symmetric with respect to a change in the Poincaré section. This will be explained in next section. The stable and unstable manifolds of hyperbolic orbits play the role of forming boundaries between qualitatively different fluid particle trajectories. In this case, trajectories that enter the wake cavity are distinct from trajectories in the upper and lower wake in that the horizontal velocity component of trajectories in the wake cavity changes sign. This is an unambiguous criterion for determining which fluid particles are “trapped” behind the cylinder.

3.3 Turnstiles and Flux

Now we can consider the question of fluid exchange between the different regions defined by our chosen boundaries that are shown in Fig. 4. The key point here is that the stable and unstable manifolds forming the boundaries of these regions quantitatively describe the exchange, and it is this feature that we now describe.

First, we list two rules that points on the stable and unstable manifolds of saddle-type fixed points must obey under iteration by the Poincaré map. (By “iteration” we mean repeated application of the Poincaré map to a particle or, in other words, discrete time evolution of a particle trajectory.)

1. A point that is on *both* the stable and unstable manifolds must remain on both manifolds under all positive and negative iterations of the Poincaré map. This is because these manifolds are *invariant manifolds*.
2. Points on the stable or unstable manifolds of a fixed point maintain their relative order (in the sense of distance in arclength from the fixed point) under iteration by the Poincaré map. That is, if we consider two distinct points on the stable or unstable manifold then one will be closer than the other to the fixed point in the sense of arclength along the stable or unstable manifold. If we then iterate both points, the same point will always thereafter be closer to the fixed point. The reasons for this are more technical and are related to uniqueness of particle trajectories for a given initial condition.

With these two rules in mind let us return to Fig. 4 and consider the preimages under the Poincaré map of the boundary intersection points, i.e., the backwards time evolution of these points for one period of the velocity field. These points are labelled $P^{-1}(q_1)$ and $P^{-1}(q_2)$ in the figure. By rule 1 these points still lie on both the stable and unstable manifolds, and since the manifolds are smooth curves they must wind through each other as shown in Fig. 5. Here we only describe the mechanism for transport between the upper wake and the wake cavity (transport across the “upper boundary”). The same argument applies to the boundary between the lower wake and the wake cavity.

Hence, the segments of the stable and unstable manifolds between a boundary intersection point and its preimage form two *lobes* and these two lobes are said to form a *turnstile*. The turnstiles are the mechanisms governing transport between the different regions, as we will now argue.

Now consider the image of the turnstile lobes under the Poincaré map P (i.e., the evolution of these points for one period of the flow). Using the two rules above, as well as the fact that (for a continuous and continuously invertible map) the boundary of a set maps to the

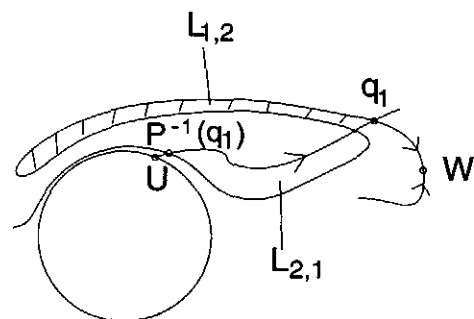
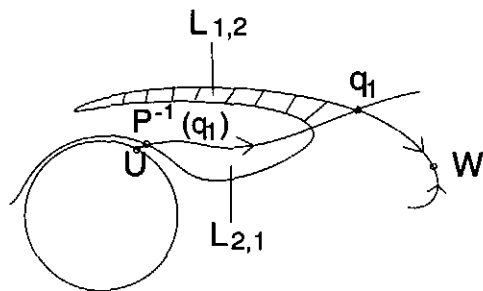


Fig. 5. $Re = 100$ (top) and $Re = 190$ (bottom):

boundary of its image and the interior of a set maps to the interior of its image, we see that the image of the turnstile lobes appear as in Fig. 6. Thus, the respective turnstile lobes have “switched sides” in relation to the boundary, hence the term “turnstile” (note: the notation for the turnstile lobes should be clear; $L_{i,j}$ denotes the turnstile lobe contained in R_i that enters R_j under iteration by P). Now, using rule 2 above, it can be argued that the *only* points that cross the boundary in one iteration of the Poincaré map are those in the turnstile lobes. Therefore the *flux across the boundary in one period* is simply the area of the turnstile lobe. More details of the theory can be found in Wiggins [1992].

In Fig. 7 we show the the turnstiles and their images for the upper boundary, and in Fig. 8 we show the turnstiles and their images for both the upper and lower boundaries.

We have computed the areas of the wake cavity and the turnstile lobes for $Re = 100$ and $Re = 190$, and the values are given in Table 1, Table 2 and Table 3, respectively.

Re	Cavity Area
100	1.14
190	0.86

Table 1 — Areas of the cavities for $Re = 100$ and $Re = 190$. The diameter of the cylinder is 1.

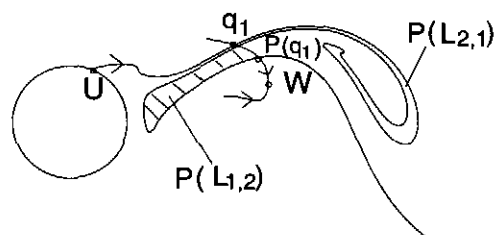
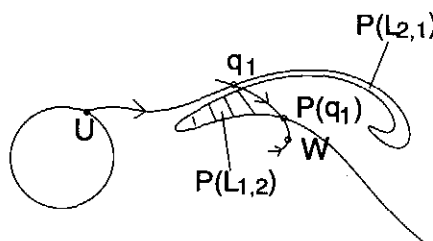


Fig. 6. $Re = 100$ (top) and $Re = 190$ (bottom):

Lobe	Area
$L_{1,2}$	0.17
$L_{2,1}$	0.17
$L_{2,3}$	0.17
$L_{3,2}$	0.17

Table 2 — $Re = 100$: Areas of the turnstile lobes. The diameter of the cylinder is 1.

Lobe	Area
$L_{1,2}$	0.17
$L_{2,1}$	0.17
$L_{2,3}$	0.17
$L_{3,2}$	0.17

Table 3 — $Re = 190$: Areas of the turnstile lobes. The diameter of the cylinder is 1.

The fact that the area of lobe $L_{i,j}$ equals the area of lobe $L_{j,i}$ indicates that the velocity field obtained through interpolation by bicubic splines preserves incompressibility, to the degree of precision to which the turnstile lobes agree in area.

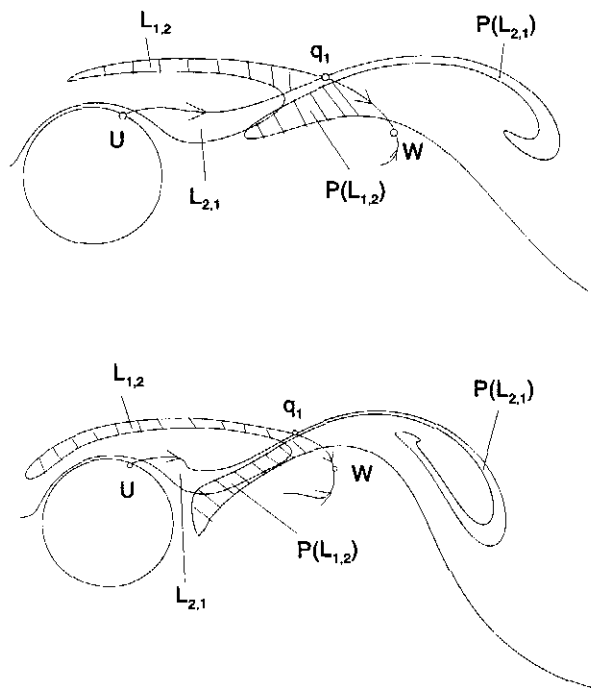


Fig. 7. $Re = 100$ (top) and $Re = 190$ (bottom): The turnstiles for the upper boundary. Hatched regions map to hatched regions.

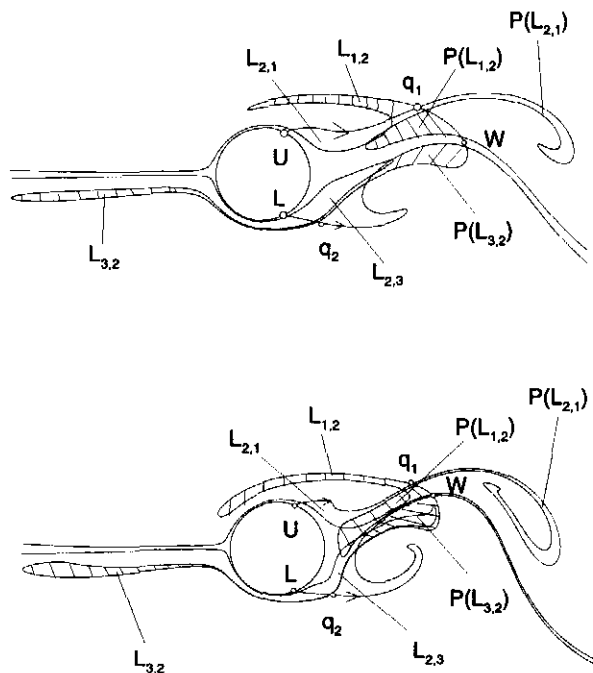


Fig. 8. $Re = 100$ (top) and $Re = 190$ (bottom): The turnstiles controlling exchange between the upper wake (R_1), the wake cavity (R_2), and the lower wake (R_3). Hatched regions map to hatched regions.

3.4 Quantifying Transport in the Near Wake

Using lobe dynamics we can describe in detail a number of features related to transport into and out of the wake cavity, and transport cross the wake cavity.

3.4.1 Symmetry with Respect to the Choice of Poincaré Section

We note that there is a symmetry with respect to the phase of the shedding cycle that is used in the choice of the Poincaré section. The velocity field $u(x, y, t), v(x, y, t)$ is computed at 51 time units with equal time-step size, i.e., we have 51 frames of values for u, v , during one shedding cycle. The Poincaré sections can be taken at any of these 51 frames. When it is taken at frame 1, we say that the Poincaré section has base phase 1, etc. There is a symmetry for the stable and unstable manifolds on Poincaré sections in the following sense. When we change the base phases of the Poincaré sections, the unstable manifold of the upper cylinder saddle point U , $W^u(U)$, will become the flip (or mirror) image of the unstable manifold of the lower cylinder saddle point L , $W^u(L)$, at an earlier (or later) base phase. See Fig. 9 for the case $Re = 100$. We note that, $W^u(U)$ at base phase 25 becomes (approximately) the mirror image of $W^u(L)$ at base phase 1.

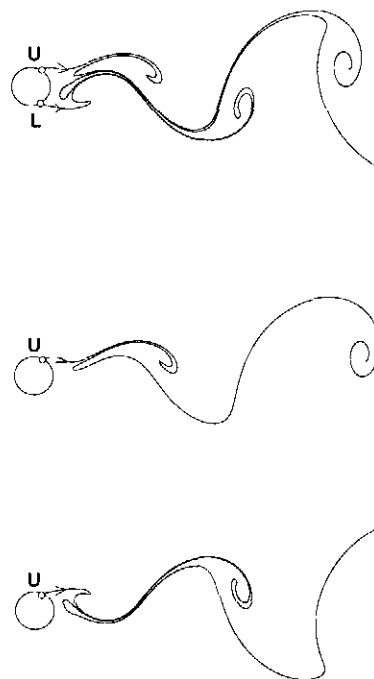


Fig. 9. $Re = 100$: The unstable manifolds of the upper and lower cylinder saddle points U and L , at base phase 1 (top); The unstable manifold of the upper cylinder saddle point U , at base

In the following we will fix the Poincaré section at the base phase 1 and, consequently, we will only need to study the transport across the upper boundary of the wake cavity.

3.4.2 Cross Wake Transport

In this section, we consider transport across the wake. We note first that

Particle trajectories can pass from the upper wake to the lower wake (or vice versa) only by making an intermediate passage through the wake cavity.

This is seen as follows: outside the cylinder and wake cavity the boundary between the upper and lower wake is the stable manifold of the saddle point M at the front of the cylinder and the unstable manifold of the saddle point W in the wake; see Fig. 10. Since trajectories cannot cross these invariant manifolds the only way a trajectory can pass from the upper to the lower wake (or vice versa) is by passing through the wake cavity.

It follows directly from our discussion of the turnstiles as the mediators of transport into and out of the wake, that the region

$$P^n(L_{1,2}) \cap L_{2,3} \quad (3)$$

consists of particles that enter the wake cavity from the upper wake, spend n shedding cycles in the wake cavity, and exit the wake cavity into the lower wake on the $n+1$ shedding cycle. (one can obtain a similar expression for transport between the lower wake and the upper wake simply by switching the 1 with the 3 in this expression.) However, we find that within the wake cavity there is a barrier that strongly inhibits this “cross-wake” transport (this was also noticed by Shariff et al. [1991]). In Fig. 10 (top) for $Re=100$ the stable manifold of the saddle point on the cylinder M appears to nearly coincide with one branch of the unstable manifold of the saddle point in the wake W . Using solely numerical methods we cannot be certain that these manifolds coincide (and thus split the wake cavity into two disjoint regions) however we can verify that in this case (3) is the empty set for $n = 1, 2, 3$. Nevertheless, even if they do not coincide it is clear that transport across the wake cavity is extremely slow, and we are able to make a qualitative comparison between the cases of $Re = 100$ and $Re = 190$.

For $Re=190$ the situation is very different. In this case the same stable and unstable manifolds intersect and exhibit large amplitude intersections as shown in the lower figure in Fig. 10 (bottom). In this figure the stable manifold of M is denoted by the dotted line and the unstable manifold of W is denoted by the solid curve. The “large amplitude” oscillations of these two manifolds are apparent in comparison to the upper figure in Fig. 10.

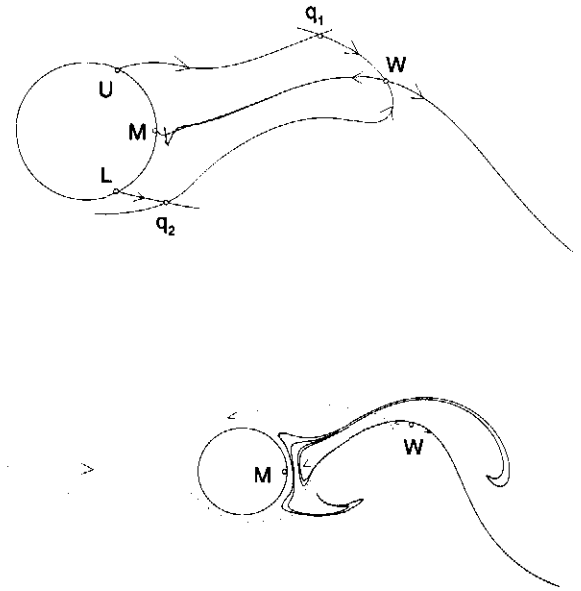


Fig. 10. $Re = 100$ (top) and $Re = 190$ (bottom): Crosswake transport.

This leads to greatly enhanced cross-wake transport as we can easily verify that (3) is nonempty for $n = 1$. This implies that particles can pass from the upper to the lower wake in one shedding cycle. This cannot happen for $Re=100$.

3.4.3 Residence Time and Escape Rates

We now consider the following problem:

If a particle enters the wake cavity from the upper wake, how long will it remain inside, and when it exits, does it enter the upper or lower wake?

This question can also be answered in terms of the turnstile lobes. The only particles that enter the wake cavity from the upper wake during each shedding cycle are those in the lobe $L_{1,2}$. Once inside the wake cavity, they can exit into the upper wake only through the lobe $L_{2,1}$, and into the lower wake only through the lobe $L_{2,3}$. Thus

$$P^n(L_{1,2}) \cap L_{2,1}, \quad (4)$$

is the set of particles that enter the wake cavity from the upper wake, spend n shedding cycles in the wake cavity, and exit the wake cavity into the upper wake; recall Fig. 7. Similarly,

$$P^n(L_{1,2}) \cap L_{2,3}, \quad (5)$$

is the set of particles that enter the wake cavity from the upper wake, spend n shedding cycles in the wake cavity, and exit the wake cavity into the lower wake. In Fig. 11 we show $P^n(L_{1,2}) \cap L_{2,1}$ for $n = 1, 2, 3$, for $Re = 100$. For $Re = 100$, $P^n(L_{1,2}) \cap L_{2,3}$ is empty for $n = 1, 2, 3$ and hence, particles that enter the wake cavity from the upper wake can only exit the wake cavity through the upper cavity boundary and enter the upper wake.

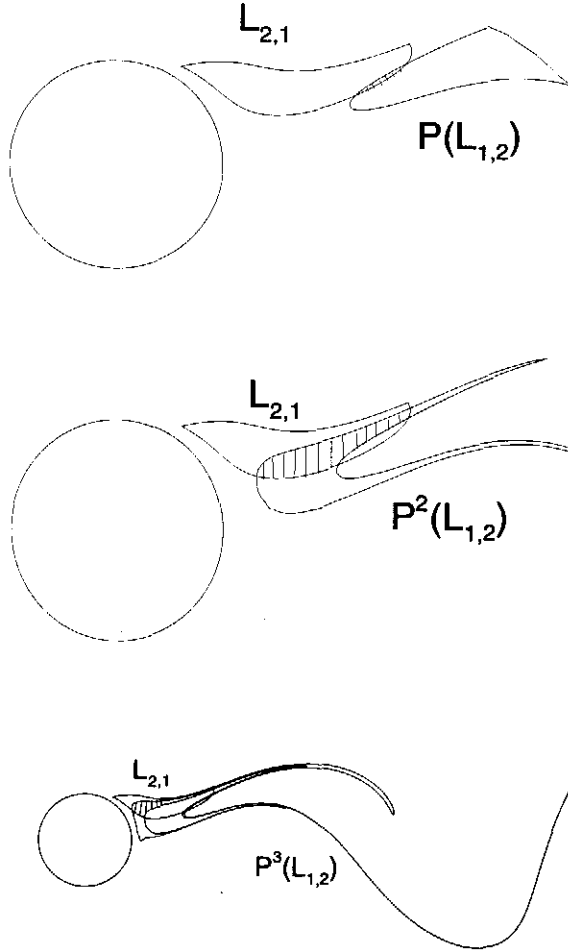


Fig. 11. $Re = 100$ — Images of the entrained lobe $L_{1,2}$.

For $Re = 100$, we have numerically computed the area of $P^n(L_{1,2}) \cap L_{2,1}$ divided by the area of the lobe $L_{1,2}$, $n = 1, 2, 3, \dots$. This describes the percentage of particles entrained into the wake cavity from the upper wake

that escape the cavity after 1, 2, and 3 shedding cycles, respectively. We refer to these quantities as escape rates of those particles entrained from the upper wake. See Table 4. For $Re = 190$, since particles entrained from the upper wake may exit into both the upper or lower wake, i.e., the images of the entrained lobe $L_{1,2}$ may intersect both lobes $L_{2,1}$ and $L_{2,3}$, the escape rates are given by the area of $(P^n(L_{1,2}) \cap L_{2,1}) \cup (P^n(L_{1,2}) \cap L_{2,3})$ divided by the area of the lobe $L_{1,2}$, $n = 1, 2, 3, \dots$. See Table 5.

Shedding Cycles	Escape Rate
cycle 1	2%
cycle 2	39%
cycle 3	30%

Table 4 — $Re = 100$: Percentage of particles entrained from the upper wake that escape on subsequent shedding cycles.

Shedding Cycles	Escape Rate
cycle 1	49%
cycle 2	41%

Table 5 — $Re = 190$: Percentage of particles entrained from the upper wake that escape on subsequent shedding cycles.

The fact that our flow is an open flow (and fluid particles continuously flow downstream) prevent us from computing $L_{1,2} \cap P^n(L_{2,1})$ for large n since the lobes relatively quickly leave the computational domain. Nevertheless, we readily see from these tables that most particles entrained into the wake cavity spend little time in the cavity before escaping. From the above tables, we see that the escape rates (hence the fate of trapped particles) are quite different for $Re = 100$ and $Re = 190$.

Now we consider the problem.

Can escaped particles re-enter the wake cavity?

The set

$$P^n(L_{2,1}) \cap L_{1,2}, \tag{6}$$

consists of particles that exit the wake cavity into the upper wake, spend n shedding cycles in the upper wake, and enter the wake cavity on the $n + 1$ shedding cycle; see Fig. 7 and Fig. 12. Numerically we find that the set (6) is empty for $Re = 100$ for $n = 1, 2, 3$, and for $Re = 190$ for $n = 1, 2$. For larger n , we would need to do computations on even larger domains. However, It seems reasonable that this is true for all n . We argue

in the following way. The lobes $P^n(L_{2,1})$ extend downstream (see Fig. 7 and Fig. 2) and this is also seen to be true in experiments (e.g., Perry et al. [1982] and references therein). Hence particles in the lobes $P^n(L_{2,1})$ do not re-enter the cavity *through the upper boundary*. On the other hand, the unstable manifold of the saddle W also extends downstream (see Fig. 12) and the lobes $P^n(L_{2,1})$ can not intersect the unstable manifold of W , since unstable manifolds can not intersect unstable manifolds. This implies that the lobes $P^n(L_{2,1})$ can not cross the unstable manifold of W , and therefore they can not intersect the turnstile lobe $L_{3,2}$ that entrains fluid into the wake cavity from the lower wake. (see Fig. 8 and Fig. 2). and hence particles in the lobes $P^n(L_{2,1})$ do not re-enter the cavity *through the lower boundary* either. Therefore we conclude that particles or trajectories that exit the wake cavity can never re-enter the wake cavity.

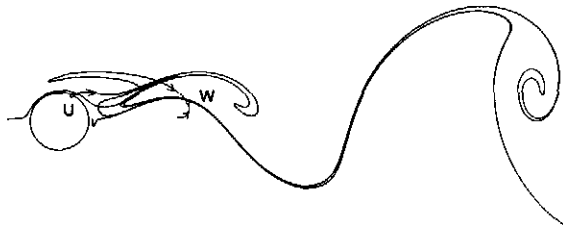


Fig. 12. $Re = 100$: Escaped particles never return. This figure shows the unstable manifold of U , and both stable and unstable manifolds of W .

4 Chaos and Stretching

In this section, we discuss the issue of chaotic particle motions in the near wake. The usual way of showing the existence of chaotic particle trajectories is to show that the stable and unstable manifolds of some hyperbolic periodic trajectory intersect transversely. Then, by the Smale-Birkhoff homoclinic theorem, one has the existence of an invariant Cantor set of fluid particle trajectories on which the dynamics is equivalent to a Bernoulli shift. This approach cannot be used here since the saddle points on the cylinder are not hyperbolic. Nevertheless, the techniques that are used to prove the Smale-Birkhoff homoclinic theorem, namely the Conley-Moser conditions (Wiggins [1990]) do not require hyperbolic-

ity. The Conley-Moser conditions are a set of sufficient conditions for a two-dimensional map to have chaotic orbits. We will not provide a mathematically rigorous proof of this here. Rather, we will show that one can track regions of fluid particles that behave like a “Smale horseshoe map”.

We pick a “rectangular” region R inside the wake cavity, see Fig. 13, and follow its evolution under the Poincaré map P .

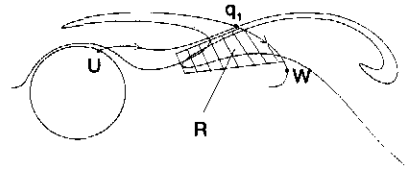


Fig. 13. ($Re = 100$): A rectangular region R whose time evolution gives rise to a horseshoe map.

In Fig. 14 we draw (based on numerical simulations) the topologically correct images of R under P , $P(R)$ and $P^2(R)$. Clearly we notice the strong folding, contraction

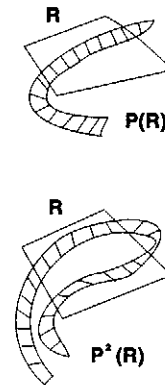


Fig. 14. Chaotic particle motions ($Re = 100$): A rectangular region R and its images under two successive iterations of the Poincaré map P

and expansion. More specifically, we can verify that P^2 maps R to a subset in the near wake and, in particular, P^2 maps two appropriately chosen vertical strips into two horizontal strips (for definition of such strips, see Wiggins [1990]), while strongly contracting in the vertical direction and expanding in the horizontal direction. By the Conley-Moser theorem, we can conclude that the (composed) map P^2 is chaotic on an invariant set Λ inside the region R , in particular, P^2 has chaotic tra-

jectories inside Λ . Therefore, some fluid particles inside the wake cavity wander around and visit large portion of the cavity purely due to convection (without molecular diffusion). While in the upper wake and lower wake, most particles (as long as they do not enter the wake cavity via turnstile lobes) will have regular trajectories pretty much like in the case of a steady wake.

The same analysis can be carried out for the lower part of the wake.

5 Conclusions

In this paper, we have used transport theory from dynamical systems theory to study the transport in the near wake of a cylinder in the two-dimensional, time-periodic regime. These techniques allow us to describe transport at a very detailed level. Most importantly, these methods can be used in conjunction with modern computational fluid dynamics methods.

We remark that the techniques described in this paper have recently been extended to two-dimensional velocity fields having aperiodic time dependence (Malhotra and Wiggins [1997]).

Appendix: Computation of Lobe Areas

In this appendix we make a few remarks concerning the numerical computation of the lobe area, as well as the accuracy of the computation.

We essentially use the trapezoidal rule to compute the lobe areas. To compute the area of a lobe (or the wake cavity), we begin by inscribing a polygon inside the lobe. Practically this is done by choosing many points along the lobe boundary, and connecting these points with line segments to obtain the polygon. We then compute the area of the polygon which gives us the approximate area of the lobe. If we denote the points chosen in this way on the boundary of the lobe by (x_i, y_i) , $i = 1, 2, \dots, k$ (the vertices of the polygon), then the area of the polygon is (cf. Zwillinger [1996, p.270]):

$$S = \frac{1}{2} ((x_1 y_2 - x_2 y_1) + \dots + (x_{k-1} y_k - x_k y_{k-1}) + (x_k y_1 - x_1 y_k)),$$

and S is positive if the increasing indices correspond to traversing the boundary of the lobe in a counterclockwise sense.

We need to take many points (vertices) to get a better approximation of lobe area by polygon area. In the actual computation, we use various polygons (with various numbers of different vertices) to approximate a given lobe until we get the same or almost the same area. This method of computing lobe area is of course not exact. If we let

$$h \equiv \max_i \sqrt{(x_{i+1} - x_i)^2 + (y_{i+1} - y_i)^2},$$

then it can be shown (Press et al. [1992]) that the error is $\mathcal{O}(h)$ as $h \rightarrow 0$. In particular, the method does converge to the exact answer as $h \rightarrow 0$.

In our situation we have another check of the accuracy of the lobe areas. By incompressibility, the lobes $L_{1,2}, L_{2,1}, L_{2,3}, L_{3,2}$ should all have same area.

Acknowledgments. We would like to thank Paul Fischer for discussions regarding the spectral element methods, Ron Henderson for help in generating the velocity fields and Karim Shariff for discussions in particle tracking and graphics programming.

6 References

- Aref, H. and M. S. El Naschie (eds.) [1994] Chaos Applied to Fluid Mixing. *Chaos, Solitons, and Fractals*, 4(6), 1-380.
- Babiano, A. Provenzale, A. and A. Vulpiani (eds.) [1994] Chaotic Advection, Tracer Dynamics, and Turbulent Dispersion. Proceedings of the NATO Advanced Research Workshop and EGS Topical Workshop on Chaotic Advection, Conference Centre Seren di Gavo, Italy, 24-28 May 1993. *Physica D76*, 1-329.
- Barkley, D. and R. D. Henderson [1995] Three-dimensional Floquet stability analysis of the wake of a circular cylinder. submitted to *J. Fluid Mech.*, 1995.
- Dennis, S. C. R. and G. Z. Chang [1970] Numerical solutions for steady flow past a circular cylinder at Reynolds numbers up to 100. *J. Fluid Mech.* 42, 471-489.
- Fischer, P. F. [1989] Spectral element solution of the Navier-Stokes equations on high performance distributed-memory parallel processors. Ph.D. thesis, MIT.
- Henderson, R. D. [1994] Unstructured spectral element methods: Parallel algorithms and simulations. Ph.D. thesis, Princeton University.
- Henderson, R. D. and G. E. Karniadakis [1995] Unstructured spectral element methods for simulation of turbulent flows. *J. Comp. Phys.* 122(2), 191-217.
- Malhotra, N. and S. Wiggins [1997] Geometric Structures, Lobe Dynamics, and Lagrangian Transport in Flows with Aperiodic Time-Dependence, with Applications to Rossby Wave Flow. to appear in the Journal of Nonlinear Science.
- Mezić, I. and S. Wiggins [1994] On the Dynamical Origin of Asymptotic t^2 Dispersion of a Non-Diffusive Tracer in Incompressible Laminar Flows, *Physics of Fluids A*, 6(6), 2227-2229.
- Mezić, I., Brady, J.F., Wiggins, S. [1996] Maximal effective diffusivity for time periodic incompressible fluid flows. *SIAM Journal of Applied Mathematics*, 56(1), 40-56.
- Patera, A. T. [1984] A spectral element method for fluid dynamics: Laminar flow in a channel expansion. *J. Comp. Phys.*, 54, 468-488.
- Press, W.H., Teukolsky, S. A., Vetterling, W.T., and B. P. Flannery [1992] *Numerical Recipes in C, second edition*. Cambridge University Press: Cambridge.
- Perry, A. E., M. S. Chong and T. T. Lim [1982] The vortex-shedding process behind two-dimensional bluff bodies. *J. Fluid Mech.* 116, 77-90.
- Shariff, K., T. Pulliam, and J. Ottino [1992] A dynamical systems analysis of kinematics in the time-periodic wake of a circular cylinder. In *Vortex Dynamics and vortex methods* (ed. C. Anderson and C. Green-gard), *Proc. AMS-SIAM Conf., Lectures in Applied Mathematics*. American Mathematical Society: Providence.
- Van Dyke, M. [1982] *An album of fluid motion*. The Parabolic Press, Stanford, 1982.
- Wiggins, S. [1990] *Introduction to Applied Non-linear Dynamical Systems and Chaos*. Springer-Verlag: New York, Heidelberg, Berlin.
- Wiggins, S. [1992] *Chaotic Transport in Dynamical Systems*. Springer-Verlag: New York, Heidelberg, Berlin.
- Zwillinger, D. (ed.) [1996] *CRC Standard Mathematical Tables and Formulae*, CRC Press, 30th Edition.